Development of a ReaxFF Reactive Force Field for Ettringite and Study of its Mechanical Failure Modes from Reactive Dynamics Simulations

Lianchi Liu,[†] Andres Jaramillo-Botero,*,[‡] William A. Goddard, III,*,[‡] and Huai Sun[†]

[†]Computational Chemistry Group, School of Chemistry and Chemical Engineering, Shanghai Jiao Tong University, 800 Dongchuan Road, Min Hang, Shanghai 200240, China

[‡]Materials and Process Simulation Center (MC 139-74), Chemistry and Chemical Engineering Division, California Institute of Technology, 1200 East California Boulevard, Pasadena, California 91125, United States

Ⓢ *Supporting Information*

ABSTRACT: Ettringite is a hexacalcium aluminate trisulfate hydrate mineral that forms during Portland cement hydration. Its presence plays an important role in controlling the setting rate of the highly reactive aluminate phases in cement paste and has also been associated with severe cracking in cured hardened cement. To understand how it forms and how its properties influence those of hardened cement and concrete, we have developed a first-principles-based ReaxFF reactive force field for Ca/Al/H/O/S. Here, we report on the development of this ReaxFF force field and on its validation and application using reactive molecular dynamics (RMD) simulations to characterize and understand the elastic, plastic, and failure response of ettringite at the atomic scale. The ReaxFF force field was validated by comparing the lattice parameters, pairwise distribution functions, and elastic constants of an ettringite crystal model obtained from RMD simulations with those from experiments. The predicted results are in close agreement with published experimental data. To characterize the atomistic failure modes of ettringite, we performed stress−strain simulations to find that Ca−O bonds are responsible for failure of the calcium sulfate and tricalcium aluminate (C3A) column in ettringite during uniaxial compression and tension and that hydrogen bond re-formation during compression induces an increase in plastic strain beyond the material's stress−strain proportionality limit. These results provide essential insight into understanding the mechanistic role of this mineral in cement and concrete degradation, and the ReaxFF potential developed in this work serves as a fundamental tool to further study the kinetics of hydration in cement and concrete.
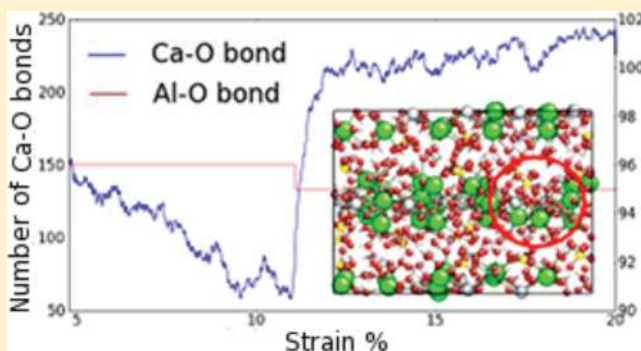
1. INTRODUCTION

The trisulfate mineral ettringite, with chemical formula $Ca_6[Al(OH)_6]_2(SO_4)_3 26H_2O$, is a precipitate formed in hydrated Portland cement as a result of the reaction of calcium aluminate (A) with calcium sulfate (C), and its presence depends on the ratio C3A. Changes in this ratio as well as the permeability of ettringite to water and its reactions with other chemical species (e.g., sulfates) affect its structural evolution during cement hydration and, consequently, cement properties. The formation of ettringite during the early cement hydration stage plays an important role in controlling the setting rate of the highly reactive aluminate phases. Its formation results in a volume increase in the fresh, plastic concrete, which has also been associated spatially with severe cracking in cured hardened concrete[1] during what is referred to as delayed ettringite formation, or DEF, and during cement degradation via sulfate attacks.[2]

To help settle the mechanistic issues, it would be most useful to understand the atomistic processes involved with mechan-ically loaded ettringite. However, the quantum mechanics (QM) methods usually applied to studies of chemical reaction processes are not capable of treating the spatial and time scales involved. Consequently, we have used QM to train the parameters of a ReaxFF[3] reactive force field and then used it to simulate the physical properties and reaction processes that occur during ettringite loading.

This paper focuses on investigating the chemical processes relevant to the mechanical properties of ettringite, including its failure modes under pressure loading, using reactive molecular dynamics (RMD). We first develop the ReaxFF first-principles-based reactive force field to describe the structures, energetics, and forces from QM on prototypical systems. Then, we carried out RMD to study the decomposition and growth of various phases over a broad set of conditions. In section 2.1.1, we

describe the ReaxFF reactive force field developed (see Supporting Information), and section 3.1 provides a description of several validation tests performed on ettringite. Then, in section 3.2, we describe how ReaxFF was used to characterize the mechanical response and failure modes of ettringite under strain loading. We consider that these modes of failure are critical to understand and control the long-term properties of Portland-based concrete structures.

2. COMPUTATIONAL DETAILS

Modern QM methods provide reaction surfaces and geometries of molecular systems sufficiently accurate to predict a reaction mechanism in advance of experiment. However, scaling of computational cost with system size (i.e., the number of atoms) limits these methods to within ~100 atoms. QM can be used to derive the forces for describing the dynamical equations of motion of all particles involved; however, again, computational costs restrict the time scale to a few picoseconds. This stems from the high cost of solving self-consistently the Schrödinger equation for all nuclear and electronic interactions. Consequently, the use of QM to study the reaction processes occurring in ettringite as the system is dynamically strain loaded/unloaded is well beyond the current practical limits of QM calculations.

2.1. ReaxFF Force Field. To provide a practical solution to such problems, we developed the ReaxFF reactive force field,[3] which provides nearly the accuracy of the best QM but at a computational cost of solving Newton's equation of motion on nuclei only. This allows us to accurately compute the atomic interactions found in ettringite. Essential elements of ReaxFF include:

1. an analytic relation between bond order and bond distance and between bond energy and bond order that establishes smooth transitions as bonds form and break
2. a rule for how charge depends on geometry and atomic character that allows charges to flow continuously as bonds form and break
3. functional forms that describe well the barrier heights of both allowed and forbidden reactions, including the effects of resonance.

ReaxFF partitions the total energy of interactions similarly to those found in nonreactive force fields like Dreiding, that is, in valence, nonbonded, and H-bond terms, but it introduces bond order dependencies on valence terms and additional potential energy corrections to properly describe bond formation and dissociation under different environmental conditions. The overall energy of the system in ReaxFF is given as

$$U_{\text{Total}} = E_{\text{bonds}} + E_{\text{angles}} + E_{\text{torsions}} + E_{\text{H-bonds}}$$
$$+ E_{\text{vdW}} + E_{\text{Coulomb}} + E_{\text{lp}} + E_{\text{over}} + E_{\text{under}}$$
$$+ E_{\text{pen}} + E_{\text{coa}} + E_{C_2} + E_{\text{triple}} + E_{\text{conj}} \quad (1)$$

where E_{lp} corresponds to the lone pair energy penalty based on the number of lone pairs around an atom, E_{over} to the energy penalty for overcoordinated atoms, E_{under} to the energy contribution for the resonance of the π-electron between attached undercoordinated atomic centers, E_{pen} to an energy penalty needed to reproduce the stability of systems with double bonds sharing an atom in a valency angle (e.g., allene), E_{coa} to the three-body conjugation term to describe the stability of $-NO_2$ groups, E_{C_2} to an energy contribution that captures

the stability of C_2, E_{triple} to a triple bond stabilization energy in CO bonded pairs, and E_{conj} to the contribution of conjugation effects to the molecular energy.

In ReaxFF, each element is described using a single atom type, even through bonding during a chemical reaction. This also facilitates the transferability of the parameters. For each element, several parameters to describe valence bond parameters, electronegativity, hardness, and other effects are optimized to reproduce the QM-derived energies and charges. ReaxFF can reproduce energies near the accuracy of the training set at a much lower computational cost. The reactive site or pathways need not be predefined in a ReaxFF MD simulation, and connectivities between the atoms are not predetermined. Instead, bond orders are calculated from the interatomic distances r_{ij}. By using a bond length/bond order relationship, smooth transitions from nonbonded to single, double, and triple bonded systems, and vice versa, are obtained. This requires bond orders to be updated every iteration, for single (σ), double (π), and triple ($\pi-\pi$) bonds as a function of interatomic distances (r_{ij}), using scaling parameters $p_{\text{BO},1-6}$ fitted from QM calculations on small representative systems and making all of the connectivity-dependent interactions bond-order-dependent to ensure that their energy contributions disappear upon bond dissociation. Bond orders are computed initially as

$$BO'_{ij} = \exp\left[p_{\text{BO},1}\left(\frac{r_{ij}}{r_0^\sigma}\right)^{p_{\text{BO},2}}\right] + \exp\left[p_{\text{BO},3}\left(\frac{r_{ij}}{r_0^\pi}\right)^{p_{\text{BO},4}}\right]$$
$$+ \exp\left[p_{\text{BO},5}\left(\frac{r_{ij}}{r_0^{\pi-\pi}}\right)^{p_{\text{BO},6}}\right] \quad (2)$$

From these (uncorrected) bond orders, BO′, an uncorrected atomic overcoordination Δ' is calculated as the difference between the total bond order around the atom and the number of its bonding electrons, Val, that is

$$\Delta'_i = -\text{Val}_i + \sum_{j=1}^{\text{neighbors}(i)} BO'_{ij} \quad (3)$$

Equation 3 is then used to obtain corrected bond orders, BO_{ij}, and subsequently a new corrected overcoordination. For more details on the exact functional forms, see the Supporting Information from ref 4.

The bond energies are then computed from the corrected bond orders by

$$E_{\text{bond}} = -D_e^\sigma BO_{ij}^\sigma \exp[p_{\text{be1}}(1 - (BO_{ij}^\sigma)^{p_{\text{be2}}})] - D_e^\pi BO_{ij}^\pi$$
$$- D_e^{\pi-\pi} BO_{ij}^{\pi-\pi} \quad (4)$$

where D_e is the corresponding dissociation energy for each bond type and $p_{\text{be1,2}}$ correspond to atomic parameters that are fitted from QM calculations on small representative cases. According to eq 4, the bond energy term E_{bond} gradually disappears as the bond order BO approaches zero during the dissociation of a bond. The ij valence angle and torsion angle energy terms are also functions of bond orders and go to zero upon bond dissociation. This ensures continuity of the energy and forces during bond dissociation/formation.

Table 1. Atom Parameters

atom type	EEM parameters			bond order correction				
	χ (eV)	η (eV)	γ (Å)	$p_{ov/un}$	p_{val3}	p_{boc4}	p_{boc3}	p_{boc5}
H	3.7248	9.6093	0.8203	−19.4571	4.2733	3.0408	2.4197	0.0003
O	8.5000	8.3122	1.0898	−3.5500	2.9000	3.5027	0.7640	0.0021
Ca	−1.7130	6.5096	1.0000	−2.0000	3.8301	49.9248	0.3370	0.0000
Al	1.7429	6.8319	0.4265	−22.7101	1.7045	20.0000	0.2500	0.0000
S	5.8284	8.2545	1.0336	−11.0000	2.7466	5.7487	23.2859	12.7147

Table 2. Bond Energy and Bond Order Parameters (D_e in kcal/mol; r in Å)

atom pair	$D_{e,\sigma}$	$D_{e,\pi}$	p_{be1}	p_{be2}	r_σ	p_{bo1}	p_{bo2}	r_π	p_{bo3}	p_{bo4}
Al−O	227.9327	0.0	−0.8375	0.3686	1.5382	−0.1740	5.2057			
S−O	161.0562	220.0	0.6070	0.7150	1.4608	−0.1109	5.4501	1.3987	−0.2741	8.3216

Nonbonded interactions (van der Waals, Coulomb) are calculated between every atom pair, irrespective of connectivity and avoiding excessive close-range contributions by shielding.

ReaxFF parameters have been developed for a variety of materials, including hydrocarbons,[3] silicon/silicon oxide,[5] metals,[6] metal oxides,[4] and metal hydrides,[7] among others. It has also been used to study a variety of complex chemical systems.[4,8−10]

2.1.1. ReaxFF Force Field for Ettringite. We developed the ettringite ReaxFF force field to accurately reproduce the first-principles QM interactions in hydrous calcium aluminum sulfate systems (H/Ca/Al/S/O) and to provide a way to extend the first-principles accuracy to the much larger length and time scales needed to examine the processes of interest here.

We started with recently derived ReaxFF parameters for Al/O from ref 11 and Ca/O from ref 12. These parameters had been optimized to describe the crystals of various phases of Al and Ca and of various aluminum oxides and calcium oxides. As discussed below, we prepared additional training data to complete the Al, Ca, O, S, and H interactions present in ettringite and validated ReaxFF charges for its constituent molecular motifs against QM Mulliken populations.

This involved performing QM density functional theory (DFT) calculations on representative finite clusters using the B3LYP hybrid functional with the LACVP** basis set using the Jaguar 4.2 package.[13] The calculations on periodic systems used the PBE functional with double-ζ plus polarization basis of contracted Gaussian functions with SeqQuest.[14] The complete QM-derived force field training set includes EOS, atomic bond energy curves, dissociation energies, angle bend energy curves, and other relevant material properties, such as heats of formation, overcoordination, and others, for all possible interactions between Ca, Al, O, S, H, and H_2O. Angle bend energies in ettringite were also trained to achieve an accurate geometrical representation of the crystal structure. These included Ca−Ca−Ca in a triangle $[Ca(OH)_2]_3$ bend to represent the potential surface of Ca−O−Ca and O−Ca−O angles, the distance of Al−Al in $Ca[AlO_4]_2$ scanned to represent the potential surface of the Ca−O−Al angle, which is typical in ettringite along the c direction, the Al−O−S angle in $Al(OH)_2$−O−SO_3H, and the Ca−O−S angle in $CaSO_4$ gas.

3. RESULTS AND DISCUSSION

The geometries and energies of the species and complexes in ettringite were calculated using DFT, and the ReaxFF force field parameters were optimized to minimize the differences between the DFT and ReaxFF energies. Tables 1−5 provide a summary of the ReaxFF force field parameters for ettringite.

Table 3. van der Waals Parameters

atom pair	R_{vdW} (Å)	ε (kcal/mol)	α	γ_{vdW}
Al−O	1.8928	0.1745	11.2476	7.3490
S−O	1.7931	0.2047	10.2391	8.2411

The corresponding ReaxFF potential functional forms may be consulted in ref 4. These optimized parameters are available in a ffield file (see the Supporting Information sectionof ref 4) that can be directly used in the freely available "Large-scale Atomic/Molecular Massively Parallel Simulator" (LAMMPS[15]) molecular dynamics program from Sandia National Laboratories.

3.1. Ettringite ReaxFF Force Field Validation. We began by constructing a 2 × 2 × 1 molecular triclinic unit supercell model from the crystal structure determined by Moore,[16] as shown in Figure 1. This molecular model served as the basic structure for the calculations reported here.

Charges play an important role in computing charge distributions and overall electrostatics during bond breaking and formation in ReaxFF. To confirm the accuracy of the net molecular charges calculated with ReaxFF (using the charge equilibration method QEq from Rappe et al[17]) on subspecies found in ettringite, including H_2SO_4, $CaSO_4$, $Al(OH)_3$, $Al(OH)_2$−O−SO_4H, and the C_3A_2 cluster, we compared these to Mulliken charge populations. Figure 2 shows that ReaxFF charges for the different species of interest are in close agreement with the QM results.

In addition to validating bond energies, EOS, and other properties, we compared DFT-calculated angle bend energies against equivalent scans using the ettringite ReaxFF force field. Angle bend energies for Ca−O−Ca, O−Ca−O, Ca−O−Al, Al−O−S, and Ca−O−S angles are important to the structural conformity of the model (see Figure 3).

To determine the structural stability and conformity of our model during room-temperature dynamics, the 2 × 2 × 1 ettringite supercell model shown in Figure 1 was equilibrated for 20 ps in an *NPT* ensemble with RMD calculations at 300 K and a 0.25 fs time step. The last 10 ps were used for statistical calculation of the cell parameters and for computing radial distribution functions (RDFs). The calculated unit cell parameters accurately reproduce the experimental values within ~4%, as shown in Table 6. The total averaged RDFs and all of the RDF pairs were also calculated (Figure 4), revealing

Table 4. Angle Parameters

angle type	$\Theta_{0,0}$ (deg)	p_{val1} (kcal/mol)	p_{val2}	p_{coa1}	p_{val7}	p_{pen1}	p_{val4}
O−Al−O	54.0864	9.7594	1.9476	0.0	3.0000	0.0	1.4400
O−O−Al	34.4326	25.9544	5.1239	0.0	2.7500	0.0	1.7141
H−O−Al	90.0000	19.7491	1.8227	0.0	1.0000	0.0	2.5337
Al−O−Al	23.7270	19.5973	4.0000	0.0	0.6619	0.0	1.9380
Ca−O−Al	79.6174	23.7025	5.7958	0.0	0.9119	0.0	1.6244
Al−O−S	102.1915	7.3381	0.4786	0.0	0.5846	0.0	1.4022
Ca−O−S	114.2370	19.7117	0.5240	0.0	3.0000	0.0	0.8335
O−S−O	81.7931	31.2043	6.5492	−4.4116	2.6067	0.0	3.0000
O−O−S	83.9753	31.0715	3.5590	0.0	0.8161	0.0	1.1776

Table 5. Torsion Angle Parameters (V in kcal/mol)

torsion angle	V_1	V_2	V_3	p_{tor1}	p_{cot1}
H−O−S−O	2.5000	2.5000	0.2237	−10.0000	−1.0000
X−O−S−X	0.1000	50.0000	0.0100	−10.0000	0.0000

predicted structures from our MD simulations that are in close agreements with experiments.

3.2. Elastic Constants of Ettringite. To characterize the stiffness of ettringite, we calculated its elastic constants from the linear relation between the stress and strain tensors in the limit of infinitesimal deformation. We computed the adiabatic constants (at 0 K) considering that the thermal expansion of the unit cell at ambient temperature, relative to that at 0 K, was within the error bars of our method (as estimated from our *NPT*-RMD structure equilibration simulations at 300 K). This involved deforming the unit cell by less than 1% in the different directions of interest and calculating the change in the corresponding stress tensor components. This way, we avoided the higher uncertainty and computational costs of calculating the elastic constants at ambient temperature, which requires time averages of differential properties (e.g., stress tensor components using a canonical or isothermal−isobaric ensemble approach) and balancing the systematic and statistical errors to fully equilibrate the deformed cell before sampling the stress tensor. Table 7 shows that the results from our simulations are quantitatively consistent with the isothermal elastic constants reported from experiments.[18]

3.3. Atomistic Failure Modes of Ettringite under Mechanical Loading. To understand the failure modes of ettringite, we carried out RMD deformation simulations, with the ReaxFF force field reported here, along the *y* and *z* directions on the model system depicted in Figure 1. We started from a relaxed volume $2 \times 2 \times 1$ supercell using *NPT*-RMD at 300 K temperature and 1 atm of pressure. The system was equilibrated at every 1% strain for 20 ps up to 15% strain in the *y* direction and 20% strain in the *z* direction, and the last 10 ps was used for data collection at each deformation strain.

The uniaxial stress−strain characteristics along the *z* direction, under compression and tension, are presented in the Figure 5. These results indicate that the true elastic limit along the *z* direction is at ∼3% under strain in compression and ∼7% in tension, while failure occurs between 11 and 12% deformation. These results also indicate that in this particular direction, ettringite is more resistant under tensile strain than under compression. We observed hydrogen bonds breaking and re-forming during compression, which accounts for the increase in plastic strain in this mode. The longitudinal elastic anisotropy due to the crystallographic structure is $C_{11}/C_{33} = 0.63$, while the shear anisotropy is $C_{66}/C_{44} = 0.6$. The stiff octahedra chains of $[Al(OH)_6]_3-$ alternating with triplets of Ca_2^+ in eight-fold coordination along the *z*-axis lead to higher stiffness in this direction.
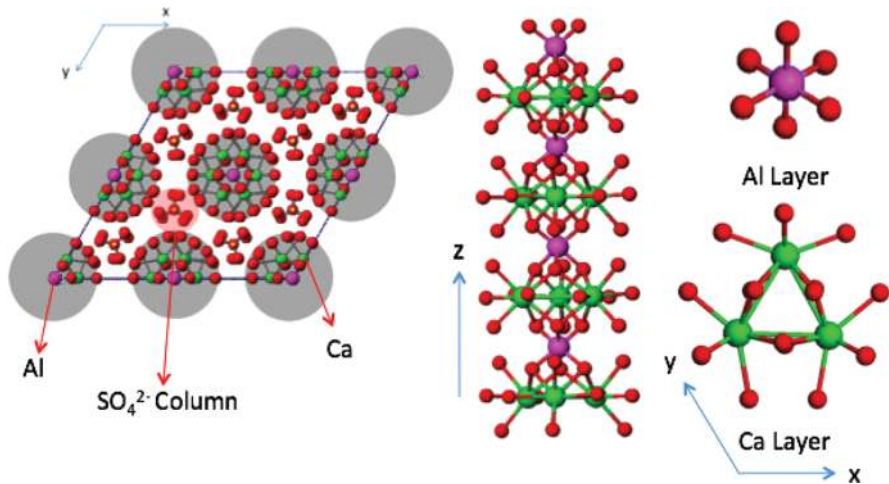

Figure 1. The triclinic $2 \times 2 \times 1$ molecular supercell crystal model of ettringite contains a total of 496 atoms, ignoring hydrogens, arranged in 4 stacked layers (center image) of intercalated Ca and Al sublayers (right image). The left image shows the projection of crystal structure on to the (0001) plane. C3A columns lay parallel to the *z*-axis (*c*) with sulfate and water molecules in the intercolumn channels. The SO_4^{2-} groups are located at the interstitials between columns, along with water molecules, and 132 hydrogen atoms (not shown) on the surface of the columns and around the SO_4^{2-} groups neutralize the system.
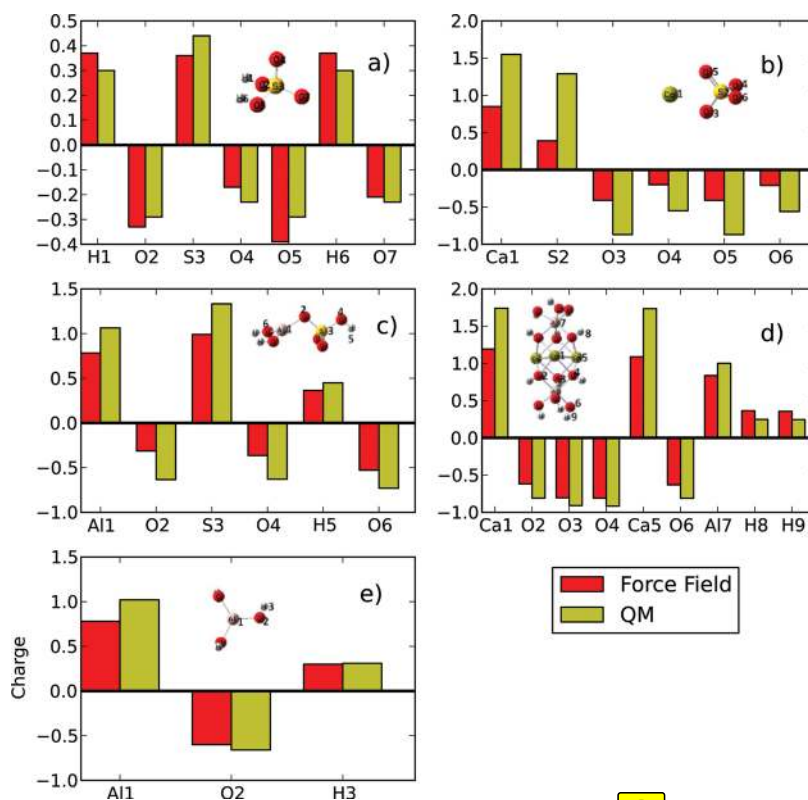
Figure 2. Comparison of the charges for Eettringite from the ReaxFF force field and from QM ...den populations for (a) H_2SO_4, (b) $CaSO_4$, (c) the C_3A_2 cluster, (d) $Al(OH)_2-O-SO_4H$, and (e) $Al(OH)_3$.
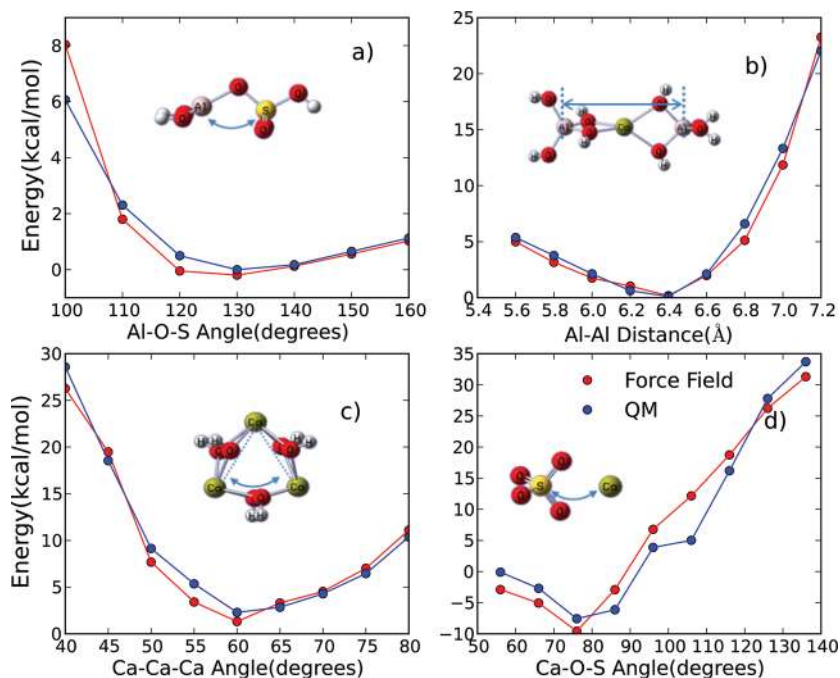

Figure 3. Comparison of the ettringite angle bend energies from ReaxFF and from QM angle scans for (a) Ca−O−Ca and O−Ca−O, (b) Ca−O−Al, (c) Al−O−S, and (d) Ca−O−S angles.

The stress−strain characteristics of the system along the y direction are shown in Figure 6. Material failure during compression in the y direction occurs at ∼13% strain and at ∼8% strain during tension. The intermolecular hydrogen bonding network that provides mechanical stability to the C3A columnar conformation are responsible for the decreased loading capacity in the a/b directions of the material.

The number of bond changes during the dynamics of mechanical strain was used to provide further insight into the failure mechanisms of ettringite.

E

Table 6. Comparison between Calculated Ettringite Cell Parameters and Experiment

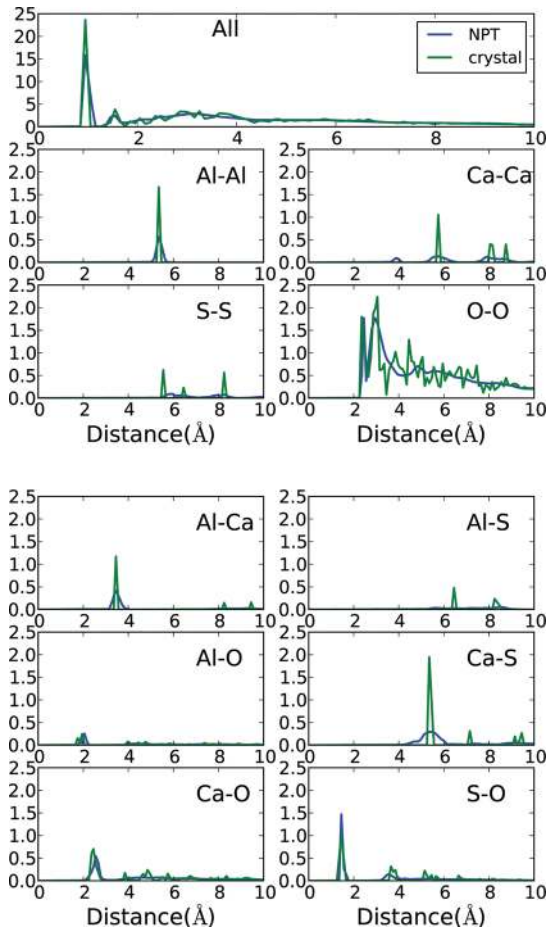| cell parameters	experimental	ReaxFF *NPT*-RMD
a/b	11.167	11.53
c	21.360	22.22

Figure 4. Radial distribution functions (RDFs) for Ettringite; experimental and ReaxFF *NPT*-RMD simulation results agree.

Figure 7 shows that during the initial stages of compression along the z direction, the number of Ca−O bonds increases slowly until ~7% compression, and they increase at a faster pace thereafter, until the failure point (~11% strain). On the

Table 7. Computed (Adiabatic) versus Experimental (Isothermal) Elastic Constants in Ettringite Crystal[a]

elastic constants	expt[18]	ReaxFF
C_{11}	35.1 ± 0.1	45.4
C_{12}	21.9 ± 0.1	25.0
C_{13}	20.0 ± 0.5	23.0
C_{14}	0.6 ± 0.2	1.9
C_{33}	55 ± 1	53.9
C_{44}	11.0 ± 0.2	11.1
C_{66}	6.6* ± 0.1	8.1
bulk modulus (K)	27.3 ± 0.9	26.76
shear modulus (G)	9.5 ± 0.8	12.44
Poisson ratio(v)	0.34 ± 0.02	0.30

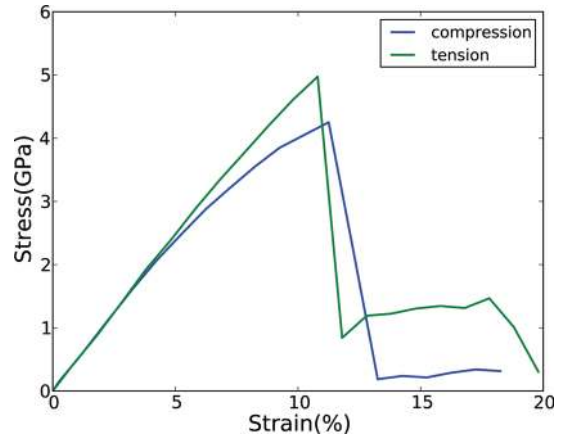[a]Note: C_{66}* is calculated as $(C_{11} - C_{12})/2$.

Figure 5. Stress−strain curve along the z direction under compression and tension deformation.
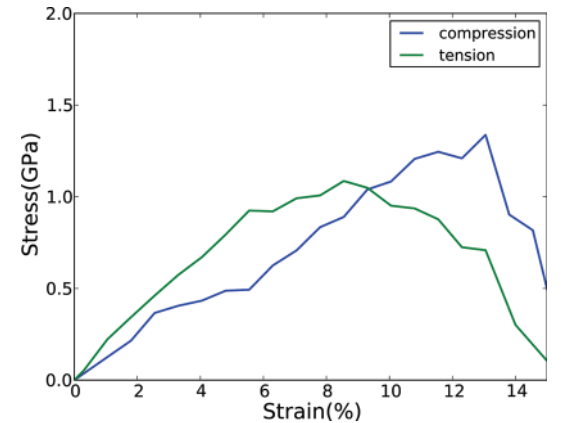

Figure 6. Stress−strain curve along the y triclinic (a/b) direction under compression (blue) and tension (black).
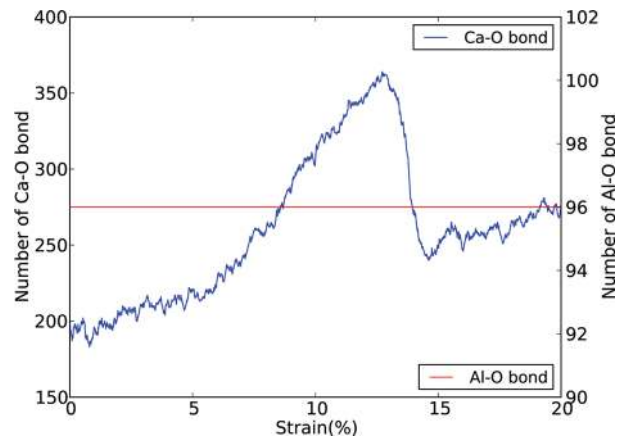

Figure 7. The number of Ca−O bonds increases piecewise linearly between 0 and 7% and 7 and 11%, until failure at ~11% elongation in the z direction, while the number of Al−O bonds remains constant during the full range of compression deformation in the same direction.

other hand, the numbers of Al−O bonds do not change during compression; therefore, the failure in this mode is attributed to Ca−O bond breaking in the C3A column. We observe that during tension, the number of Ca−O bonds decreases at a constant rate before reaching the failure point of the material, at ~11% tension, and sharply increases thereafter (Figure 8). The

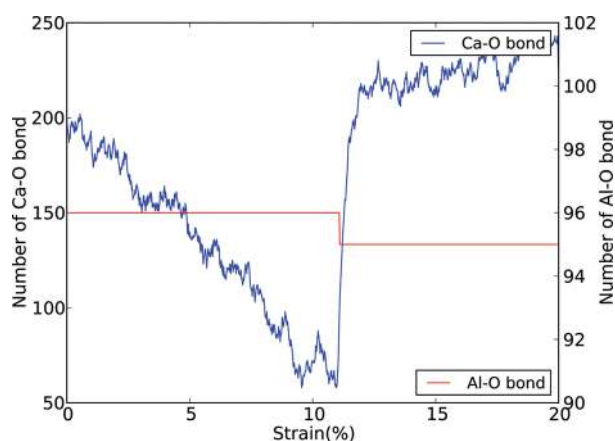**Figure 8.** The number of Ca−O bonds decreases linearly during elongation in the z direction until failure at ∼11%, while the number of Al−O bonds decreases by one at the failure point.
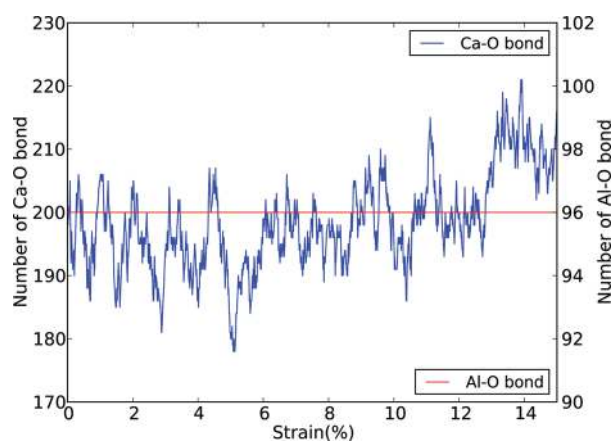
C3A column loses its structural character after one Al−O bond is lost, which occurs after the system's failure point at ∼11% elongation.

From Figures 7 and 8, it is evident that the change in the number of Ca−O bonds is much less than that observed for the z (c) direction. Moreover, these changes are mainly due to the Ca−water interactions because the conformation of the C3A column is not changed during the deformation. The failure mechanism in this case is associated with hydrogen bond breaking between neighboring C3A columns.

The monocline structure in ettringite, which causes some shear stress, and hydrogen bond breaking are responsible for the oscillatory nature of Figures 9 and 10.
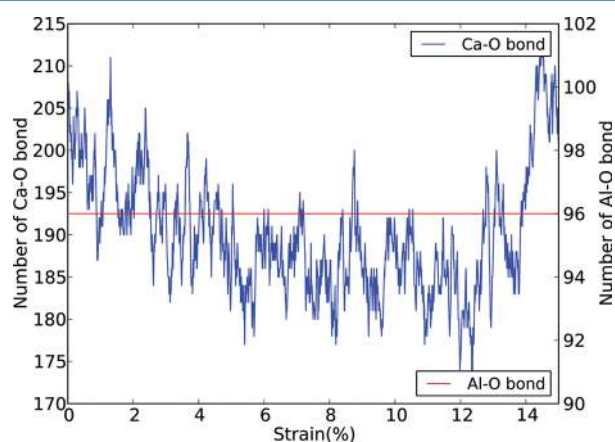

Figure 9. The number of Ca−O bonds decreases linearly during compression in the y triclinic direction, and a small increase is observed after failure at ∼12%, while the number of Al−O bonds remains constant even after the failure point.

4. SUMMARY AND CONCLUSIONS

We have developed and validated a first-principles-derived ReaxFF reactive force field for ettringite and applied it to study the general mechanical properties and atomistic failure mechanisms of the ettringite mineral. In particular, we determined the structural stability and geometry of ettringite at ambient temperature to be in close agreement with

Figure 10. The number of Ca−O bonds changes little during tensile deformation in the y triclinic direction, with a slight increase after failure at ∼12%.

experimental RDFs, its adiabatic elastic constants to be in quantitative agreement with experimentally obtained constants, and from isothermal−isobaric RMD simulations, the sequence of molecular events that lead to its failure under mechanical compression and tension. We found that Ca−O bond breaking in the C3A column leads to failure during compression and tension, while hydrogen bond network formation leads to an increase in plastic strain during compression.

The results presented here are essential for understanding the role of ettringite in cement and concrete properties. We are now using this ReaxFF force field to study the hydration kinetics of ettringite and the effect of water on ettringite (and delayed ettringite formation, DEF) as it pertains to the long-term degradation of cement paste and concrete properties. This will be the subject of a subsequent publication.

■ ASSOCIATED CONTENT

ⓢ Supporting Information

Description of the ReaxFF reactive force field developed. This material is available free of charge via the Internet at http://pubs.acs.org.

■ AUTHOR INFORMATION

Corresponding Author
*E-mail: ajaramil@caltech.edu (A.J.-B.); wag@wag.caltech.edu (W.A.G.).

Notes

The authors declare no competing financial interest.

■ ACKNOWLEDGMENTS

■ REFERENCES

(1) Lee, H.; Cody, R. D.; Cody, A. M.; Spry, P. G. *Environ. Eng. Geosci.* **2003**, *9*, 313−326.

(2) Santhanam, M.; Cohen, M. D.; Olek, J. *Cem. Concr. Res.* **2001**, *31*, 845−851.

(3) van Duin, A. C. T.; Dasgupta, S.; Lorant, F.; Goddard, W. A. *J. Phys. Chem. A* **2001**, *105*, 9396−9409.

(4) Chenoweth, K.; A.C.T., v. D.; P., P.; Cheng, M.; J., O.; W.A., G. I. *J. Phys. Chem. C* **2008**, *112*, 14645−14654.

(5) van Duin, A. C. T.; Strachan, A.; Stewman, S.; Zhang, Q. S.; Xu, X.; Goddard, W. A. *J. Phys. Chem. A* **2003**, *107*, 3803−3811.

(6) Zhang, Q.; Cagin, T.; van Duin, A.; Goddard, W. A.; Qi, Y.; Hector, L. G. *Phys. Rev. B* **2004**, *69*, 11.

(7) Cheung, S.; Deng, W. Q.; van Duin, A. C. T.; Goddard, W. A. *J. Phys. Chem. A* **2005**, *109*, 851−859.

(8) Chenoweth, K.; Cheung, S.; van Duin, A. C. T.; Goddard, W. A.; Kober, E. M. *J. Am. Chem. Soc.* **2005**, *127*, 7192−7202.

(9) van Duin, A. C. T.; Zeiri, Y.; Dubnikova, F.; Kosloff, R.; Goddard, W. A. *J. Am. Chem. Soc.* **2005**, *127*, 11053−11062.

(10) Nielson, K. D.; van Duin, A. C. T.; Oxgaard, J.; Deng, W. Q.; Goddard, W. A. *J. Phys. Chem. A* **2005**, *109*, 493−499.

(11) Kim, S.; Persson, P.; Kumar, N.; Sofo, J.; Kubicki, J.; van Duin, A. *J. Phys. Chem. A* **2011**, Submitted.

(12) Manzano, H.; Buehler, M.; Pellenq, R.; van Duin, A. In preparation for submission.

(13) *Jaguar*; Schrodinger, LLC: New York, 2011.

(14) Schultz, P. A.; Muller, P. *SeqQuest Electronic Structure Code*; Sandia National Laboratories: Albuquerque, NM, 2011.

(15) Plimpton, S. *J. Comput. Phys.* **1995**, *117*, 1−19.

(16) Moore, A. E.; Taylor, H. F. W. *Acta Crystallogra., Sect. B* **1970**, *B 26*, 386.

(17) Rappe, A. K.; Goddard, W. A. *J. Phys. Chem.* **1991**, *95*, 3358−3363.

(18) Speziale, S.; Jiang, F. M.; Mao, Z.; Monteiro, P. J. M.; Wenk, H. R.; Duffy, T. S.; Schilling, F. R. *Cem. Concr. Res.* **2008**, *38*, 885−889.